






A New AGILE MCAL Configuration to Detect Gamma-Ray Bursts and Sub-threshold Events in the Multimessenger Era

Alessandro Ursi¹ , Marco Tavani^{1,2,3,4} , Francesco Verrecchia^{5,6} , Martino Marisaldi^{7,8}, Andrea Argan¹, Alessio Trois⁹, and Patrizio Tempesta¹⁰

¹ INAF-IAPS, National Institute for Astrophysics, via Fosso del Cavaliere, 100, I-00133, Roma, Italy; alessandro.ursi@inaf.it

² Dipartimento di Fisica, Università di Roma “Tor Vergata”, via della Ricerca Scientifica 1, I-00133, Roma, Italy

³ Gran Sasso Science Institute, viale Francesco Crispi 7, I-67100 L’Aquila, Italy

⁴ Accademia dei Lincei, Palazzo Corsini, Via della Lungara, 10, I-00165, Roma, Italy

⁵ ASI Science Data Center, via del Politecnico snc, I-00133, Roma, Italy

⁶ INAF-Osservatorio Astronomico di Roma (OAR), via di Frascati, 33 I-00040, Monteporzio Catone (RM), Italy

⁷ Birkeland Centre for Space Science, Department of Physics and Technology, University of Bergen, Norway

⁸ INAF-Osservatorio di Astrofisica e Scienza dello Spazio di Bologna (OAS), National Institute for Astrophysics, via Piero Gobetti, 101, I-40129, Bologna, Italy

⁹ INAF-Osservatorio Astronomico di Cagliari (OAC), Via della Scienza 5, I-09047, Selargius (CA), Italy

¹⁰ Telespazio SpA, Centro Spaziale del Fucino, 23—Piana del Fucino, Via Cintarella, I-67050, Ortucchio (AQ), Italy

Received 2018 September 28; revised 2018 November 19; accepted 2018 November 20; published 2019 January 18

Abstract

Starting in 2016 August, the onboard software configuration of the Astrorivelatore Gamma ad Immagini LEggero (AGILE) MiniCALorimeter (MCAL) was modified in order to increase the instrument trigger capabilities for the detection of short duration high-energy transients, such as weak gamma-ray sub-threshold events and short gamma-ray bursts. MCAL is a nonimaging, all-sky detector, operating in the energy range 0.4–100 MeV. This change was carried out in order to make AGILE more competitive in the detection of electromagnetic counterparts to gravitational wave events revealed by the Laser Interferometer Gravitational-Wave Observatory/Virgo experiments. In the 22 months from 2016 August to 2018 May, the new adopted MCAL-GW configuration substantially enhanced the number of MCAL onboard triggers, increasing the total acquisition time of the instrument, and resulted in the detection of 52 bursts, 40 of which have been confirmed by the InterPlanetary Network.

Key words: gamma-ray burst: general – methods: observational

1. Introduction

1.1. Gamma-Ray Bursts (GRBs) and Sub-threshold Events (STEs)

GRBs are short duration blasts of gamma-rays, produced by ultra-relativistic particles accelerated in extra-galactic central engines, typically releasing isotropic energies $E_{\text{iso}} > 10^{51}$ erg and representing the most luminous phenomenon in the universe (Gehrels & Mészáros 2012). GRBs usually consist of an initial prompt phase, produced by the internal shocks in outflows: this phase is usually followed by a successive afterglow emission, observed in a wide range of wavelengths, generated by the interaction of jets with the surrounding environment (Mészáros & Rees 1993; Wijers et al. 1997; Piran 2003). Serendipitously discovered in the late 1960s (Klebesadel et al. 1973), these events became the target of study of a number of satellites and space missions devoted to high-energy astrophysics. GRBs are currently detected at a rate of one to two per day, and are historically classified by means of their spectrum and prompt phase T_{90} duration, defined as the time over which the central 90% of the fluence is received (Kouveliotou et al. 1993): short GRBs are bursts with $T_{90} < 2$ s, usually characterized by a hard spectrum, whereas long GRBs last $T_{90} > 2$ s up to several minutes and exhibit rather softer spectra. Such an empirical difference is a consequence of the different nature of the progenitor models: short GRBs have been recently confirmed as the product of the mergers of binary neutron stars (BNS) (Abbott et al. 2017a, 2017b, 2017c), and are thought to be produced in neutron star—black hole (NS—BH) systems as well (Belczynski et al. 2006; Nakar 2007; Baiotti & Rezzolla 2017), whereas long GRBs are clearly

associated with the collapse of Type Ic core-collapse supernovae (Galama et al. 1998). In particular, the correlation between BNS mergers and short GRBs was confirmed by the joint detection of the gravitational wave event GW170817 by the Laser Interferometer Gravitational-Wave Observatory (LIGO)/Virgo experiments and the GRB 170817A event detected by the *Fermi* Gamma-ray Burst Monitor (GBM) and the SPectrometer onboard *INTEGRAL* Anti-Coincidence Shield (SPIACS) instrument on board the INTERNATIONAL Gamma-Ray Astrophysics Laboratory (*INTEGRAL*), representing the first direct experimental evidence of a BNS system and its associated electromagnetic-gravitational radiation (Abbott et al. 2017a; Connaughton et al. 2017; Goldstein et al. 2017).

We use “STEs” to refer to weak or very short duration GRBs, that usually are not capable of triggering onboard data acquisitions, but can be identified on-ground by off-line search algorithms. Sub-threshold triggers are usually detected by several space missions, such as *INTEGRAL* (Higgins et al. 2017), *Swift* (Burns et al. 2016), and *Fermi* (Briggs et al. 2016; Kocevski et al. 2018). While a fraction of these candidate events can be confirmed by stand-alone instruments, such as the *Fermi*-GBM, others cannot be solidly assumed as genuine bursts and do not represent reliable events by themselves, but gain interest when simultaneously and independently detected by $n > 1$ satellites. It is extremely important to carefully evaluate STEs, as they can represent weak electromagnetic counterparts to gravitational wave events: the GRB 170817A detected by the *Fermi*/GBM in coincidence with the gravitational wave GW170817 detected by the LIGO/Virgo experiments (Goldstein et al. 2017) was a short GRB, simultaneously

Table 1

AGILE/MCAL Baseline and MCAL-GW Onboard Trigger Configurations, with Related Count Rate Thresholds Required to Issue Onboard MCAL Triggers, in the Hardware and Software Logic Timescales

	Hardware			Software			
	sub-ms	1 ms	16 ms	64 ms	256 ms	1,024 ms	8,192 ms
onboard trigger logic							
baseline count rate threshold	8	10	41	7σ	5σ	5σ	5σ
MCAL-GW count rate threshold	7	8	23	5σ	4σ	4σ	4σ

detected by the *INTEGRAL*/SPI-ACS as a weak brief signal made of a single excess in a 0.1 s bin, with an independent significance of 4.6σ . As a consequence, especially in the era of GW detection and multimessenger astronomy, a systematic evaluation of these sub-threshold triggers is crucial: parallel cross-checks by means of independent detectors can play a fundamental role in digging further into the background than stand-alone instruments, recovering and confirming possible high-energy transients of astrophysical interests.

Our study of MiniCALorimeter (MCAL) data in the current MCAL-GW onboard configuration started with Verrecchia et al. (2017), regarding the observations of GW170104, for which the LV trigger time was fully covered by a high time resolution MCAL data acquisition, issued by a spurious onboard automatic trigger. In this work, we address the topic of the short duration events acquired by the Astrorivelatore Gamma ad Immagini LEggero (AGILE) MCAL, whose number has substantially increased after the implementation of the MCAL-GW configuration, trying to detect and systematically characterize these events and discriminate them against background fluctuations.

1.2. The AGILE MCAL

The MCAL (Labanti et al. 2009) is one of the main detectors on board AGILE (Tavani et al. 2009). It consists of a nonimaging detector composed of 30 CsI(Tl) scintillation bars, with a total on-axis geometrical area of 1400 cm², and sensitive in the 400 keV–100 MeV energy range. MCAL can work together with the AGILE Silicon Tracker (ST), in the so-called GRID mode, providing measurements every time the ST is triggered, or in the so-called BURST mode, self-triggering transient events and acquiring data independently. The BURST mode is managed by a fully configurable onboard trigger logic (Argan et al. 2004).

The burst search logic is based on the principle that a transient phenomenon produces a count rate above a certain threshold over the background rate. As the background value strongly depends on energy and timescales, it is evaluated by using several different RateMeters (RMs), estimated on different Search Integration Time (SIT) windows, as well as on different energy ranges. Such RMs are handled by Hardware (timescales of: 0.293 ms, 1 ms, and 16 ms) and Software (timescales of: 64 ms, 256 ms, 1024 ms, and 8192 ms) logics, consisting of nine different RMs, covering three ranges of energy, respectively: Low-Energy [0.3–1.4 MeV], Medium-Energy [1.4–3 MeV], and High-Energy [3–100 MeV]. A special and unique feature of the MCAL logic is the hardware 0.293 ms, or “sub-ms,” search window, issued whenever N counts are released in a timescale of 0.293 ms: this turned out to be very suitable in the detection of extremely brief events, such as Terrestrial Gamma-ray Flashes (TGFs), lasting few hundreds of microseconds (Marisaldi et al. 2010, 2014), as well

as GRBs with exceptional high fluxes (e.g., GRB 180914B, Ursi et al., GCN #23226).

There are two different triggering methods, based on the timescale of interest and checked at periodic times depending on the SIT durations. The Burst-START signal, corresponding to the time at which the trigger acquisition begins, is issued whenever the validation criteria are passed, corresponding to two possible logics: an adaptive trigger logic, that determines the background rate B for each period of time and dynamically imposes a certain threshold $S = B + N\sigma$, with N number of standard deviations above the background (this logic works for the software trigger timescales, 64 ms, 256 ms, 1,024 ms, and 8,192 ms); a static trigger logic, that imposes a fixed threshold S (this logic works for the hardware trigger timescales, sub-ms, 1 ms, and 16 ms).

As the Burst-START is issued, MCAL data are stored in a cyclic buffer, until a valid Burst-STOP is found, corresponding to the time at which all RMs reach the normal background level and the data acquisition ends. If a Burst-STOP condition is not found, the data acquisition is forced to stop and a new background estimation is performed. Data regarding the burst are stored in the cyclic buffer, together with all events occurring in a time interval preceding (pre-burst) and following (post-burst) the trigger, and completed with other RMs from other subsystems (ST and Anti-Coincidence—AC), before being delivered to the telemetry. The trigger logic is extremely flexible: all logic parameters (background estimation time, threshold, pre- and post-burst time acquisitions) are configurable from the ground by telecommands.

2. The Enhanced MCAL-GW Configuration

Starting 2016 August, the AGILE MCAL was put into the so-called MCAL-GW configuration, which consists of a general lowering of the onboard trigger logic thresholds, in order to make the instrument more sensitive to very short and weak events. The current trigger logic threshold values for the different timescales are reported in Table 1. Static hardware trigger thresholds are now set to a minimum of 7 counts, 8 counts, and 23 counts, for the sub-ms, 1 ms, and 16 ms timescales, respectively. Dynamic software trigger thresholds are now set to a minimum of 5σ , 4σ , 4σ , and 4σ above the background rate, for the 64 ms, 256 ms, 1024 ms, and 8192 ms timescales, respectively. The duration of each acquisition window depends on the triggered logic timescale and the duration of the detected transient as well: generally, the hardware timescales trigger on very short events and last about ~ 10 s, whereas the software ones trigger on long lasting events and may acquire data for up to 30–40 s, depending on the time at which the Burst-STOP condition is encountered.

The MCAL-GW configuration includes the inhibition of the AC shield veto for MCAL, which has been implemented since

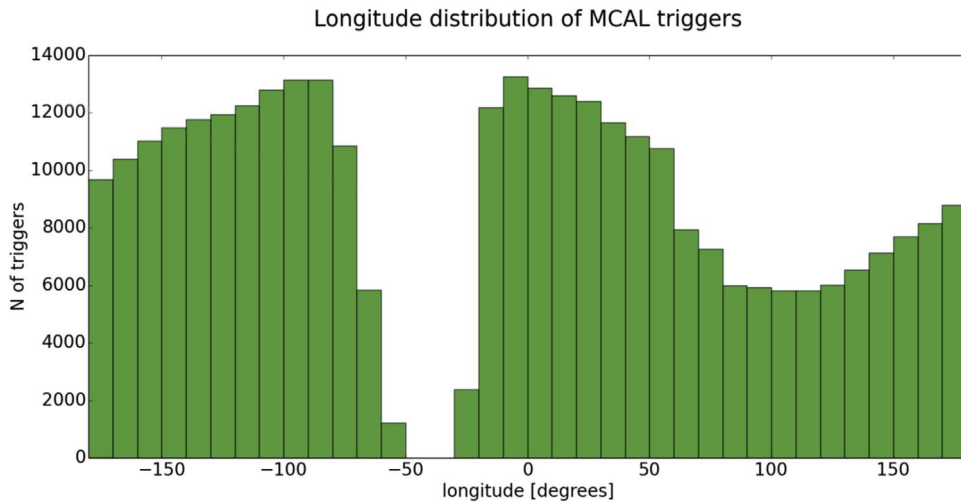


Figure 1. Longitude distribution of all MCAL onboard triggers, for all timescales. It is clear the orbital variation produced by the geomagnetic field modulation of the charged particle background, which reflects the nonuniform exposure of the instrument along the orbital path, with a larger number of triggers issued nearby the South Atlantic Anomaly (SAA), where the geomagnetic field is at its minimum.

Table 2

Onboard Hardware Logic Thresholds in the MCAL-GW Configuration and Related Significances Required for a Signal to Issue a Trigger Acquisition, over a Background Rate of ~ 580 Hz

Onboard Hardware Trigger Logic	Sub-ms	1 ms	16 ms
baseline count rate threshold	8 counts (19.0σ)	10 counts (12.4σ)	41 counts (10.4σ)
MCAL-GW count rate threshold	7 counts (16.5σ)	8 counts (9.7σ)	23 counts (4.5σ)

Note. The most favorable condition is represented by the 16 ms timescale, for which a 4.5σ significance is needed to start an onboard data acquisition, representing the mostly triggered logic timescale ($\sim 90\%$ of all onboard triggers).

2015 March to make the instrument more sensitive to short duration TGFs (Marisaldi et al. 2015). Lowering the onboard trigger thresholds and inhibiting the AC shield veto naturally exposes MCAL to the background flux of charged particles, which contributes to the overall background rate and should be carefully evaluated.

Although this change of configuration translated into a higher rate of triggers, requiring the storage of a large amount of data in the satellite’s onboard mass memory, the MCAL-GW configuration can be used for complete telemetry coverage by the AGILE ground station.

The MCAL-GW configuration increased the number of onboard triggers from about ~ 10 triggers/orbit to about ~ 60 triggers/orbit. The static nature of the hardware trigger logic makes the sub-ms, 1 ms, and 16 ms timescales react differently to the low thresholds of the MCAL-GW configuration, as shown in Table 2.

It is clear that the most favorable trigger condition is given by the 16 ms timescale, for which the corresponding threshold level required to start an onboard acquisition corresponds to a 4.5σ signal above the background rate, taken as an average 580 Hz count rate: as expected, in the new configuration, the 16 ms logic timescale is the most triggered logic timescale, representing almost $\sim 90\%$ of total onboard triggers. On the contrary, the submillisecond trigger timescale can be triggered only by extremely high-significance short duration events, corresponding to $\sim 19\sigma$, as in the case of brief bright events such as TGFs or GRBs with extremely high fluxes.

Hardware logic timescales are affected by the orbital background variation due to the geomagnetic field modulation

of the charged particle background: a larger number of triggers occur nearby the South Atlantic Anomaly, where the geomagnetic field is at its minimum, with respect to the number of triggers issued over the Indian ocean, where the field is at its maximum. On the contrary, the onboard software logics are not affected by such background variation, as they are ruled by a dynamic threshold evaluation. As a consequence, the MCAL high time resolution data total exposure is not uniform with respect to terrestrial longitude, as shown in Figure 1, but follows the geomagnetic field trend.

Aim of the MCAL-GW configuration is not only to improve the MCAL onboard trigger capabilities to the detection of weak events, by lowering the logic thresholds, but also to increase the onboard acquisition time of MCAL, in order to have the largest available fraction of data throughout each orbital revolution. This increases the probability to have weak events falling inside already triggered acquisition windows, as occurred in the case of GW170104, whose LIGO/Virgo trigger time was fully covered by an MCAL data acquisition (Verrecchia et al. 2017). Taking into consideration an average number of ~ 60 triggers acquired for each orbit, and considering that most (90%) of them consist of 16 ms hardware logic triggers lasting ~ 10 s, MCAL has currently an average acquisition time of >540 s per orbit, corresponding to about $>10\%$ data coverage.

3. The Search Algorithm

In order to search for GRBs and STEs inside the MCAL high time resolution data, an off-line algorithm has been implemented,

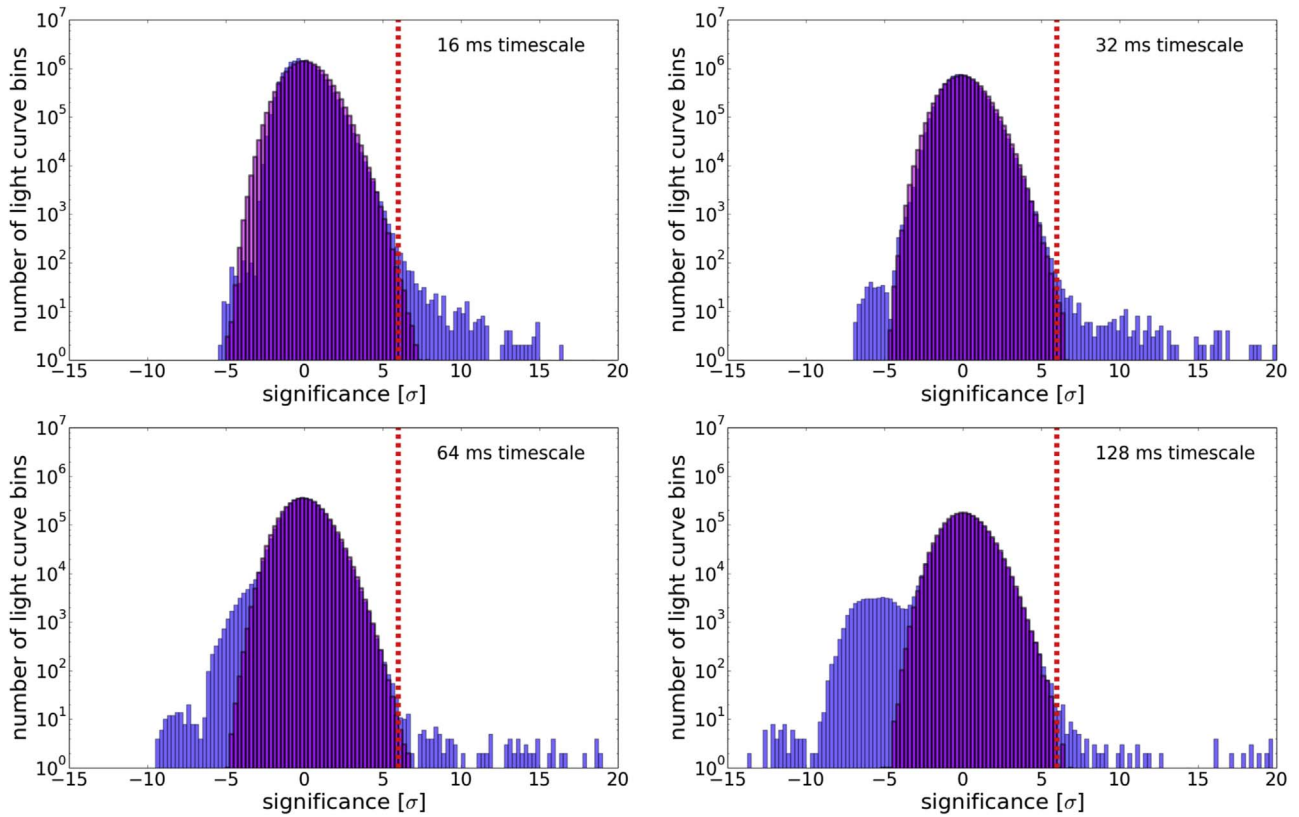


Figure 2. Distributions (blue) of the S/N of time bins of the MCAL rebinned light curves in the 16 ms, 32 ms, 64 ms, and 128 ms timescales, evaluated on a common sample of 10^6 counts. For $S/N < 6\sigma$, neglecting the negative sigmas domain ruled by non-Poissonian electronic noise, the distributions generally follow a Poisson distribution (magenta), as expected from background independent events, whereas for $S/N \geq 6\sigma$, the distributions show a tail including all events identified as STEs.

aimed at looking for short duration transients within each trigger acquisition window. The algorithm acts on four different timescales: 16 ms, 32 ms, 64 ms, and 128 ms. The significance of each light-curve bin with respect to the background rate in a given timescale is given by evaluating the number of counts in that single bin, with respect to the background rate, rebinned in that timescale as well. However, events may release counts that can be distributed in different ways throughout the light curve, depending on how the bins are centered: a high-significance event can be underestimated if its counts are split among consecutive bins. For this reason, for each timescale, four bin shifts of $+0/4$, $+1/4$, $+2/4$, and $+3/4$ of bin are evaluated at the same time, in order to consider different count distributions within the time bins. Considering four different shifts that are partially dependent on one another due to the partial overlap affects the calculation of the False Alarm Probability of these events, which should be carefully evaluated by considering four partially dependent trial search windows.

For each trigger acquisition, the average background rate is computed in the corresponding timescale and time shift under consideration. Then each time bin of the rebinned light curve is analyzed. The condition for a time bin to be identified as a candidate STE is to have a significance of $\geq 6\sigma$ above the background rate. Such a value is chosen by considering the distribution of the signal-to-noise ratio (S/N) of single light-curve bins. Figure 2 shows four plots representing the distributions (blue) of the significance of the light-curve bins in the 16 ms, 32 ms, 64 ms, and 128 ms timescales, respectively, built from a common sample of $\sim 10^6$ MCAL counts. Rebinning this number of counts in different timescales

results in different numbers of associated light-curve bins (i.e., $\sim 16 \times 10^6$ bins in the 16 ms, $\sim 8 \times 10^6$ bins in the 32 ms, $\sim 4 \times 10^6$ bins in the 64 ms, and $\sim 2 \times 10^6$ bins in the 128 ms). For each plot, we overplotted the distribution (magenta) of an equal number of simulated light-curve time bins following a Poisson distribution. Neglecting the negative sigmas regime, where a non-Poissonian electronic noise rules, bins with an $S/N < 6\sigma$ generally follow an expected Poisson distribution of a genuine background made of independent counts. On the other hand, for $S/N \geq 6\sigma$, the bin significance distributions strongly depart from a Poisson-like distribution, including all events that represent extremely low probability statistical fluctuations, thus classified as STEs. These distributions are computed adopting no time shifts, as they only serve to identify a nominal threshold for the definition of STEs. We selected the $\sim 10^6$ counts considered to build up the distributions from a data acquisition not containing GRBs or TGFs, that would have affected the S/N estimate. As the AGILE MCAL is one of the most sensitive instrument to TGFs, it is important to carry out a cross-check between the STE sample and the TGF population identified by the AGILE MCAL TGF search algorithm (Marisaldi et al. 2015), in order to exclude events of confirmed terrestrial origin. Figure 3 shows an example of a high-significance STE detected by MCAL, in the 32 ms timescale: all counts are released within a single time bin, resulting in an event with a significance of 12σ over the background rate of 17 counts/32 ms. In this case, in order to obtain the maximum significance, a time shift of $+2/4$ of bin was adopted.

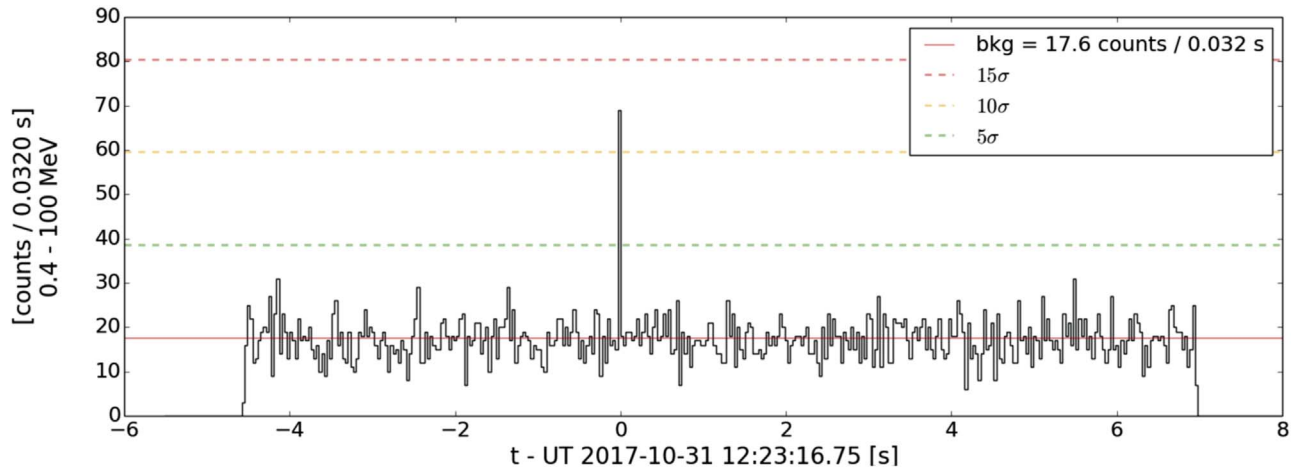


Figure 3. Example of an STE detected by MCAL and identified by the search algorithm, in the 32 ms timescale. All counts are released within a single time bin, whose reconstructed significance is 12σ over the 17 counts/bin background rate. In order to obtain the maximum significance, a time shift of $+2/4$ has been adopted.

As the AGILE AC shield veto for charged particles is turned off in the MCAL-GW configuration, it is important to carefully evaluate whether the STE sharp spikes in the light curves are produced by charged particles crossing the detector. For this reason, we focused on the single counts released inside MCAL, in order to identify signatures of particles interacting with the instrument. MCAL is composed of 30 independent scintillation bars, acquiring data in a photon-by-photon mode, with an absolute time resolution of $2 \mu\text{s}$: gamma-ray photons reaching the instrument release energy throughout the scintillation bars are detected as individual counts, each of which can be represented by its multiplicity M in the MCAL plane (i.e., the number of bars hit by the source photon) and its associated reconstructed energy E (i.e., the total energy released by that hit, nominally within 0.4–100 MeV for each bar). Usually, gamma-ray transients, such as GRBs, release a large amount of photons in a limited time interval, much larger than the MCAL absolute time accuracy, and are observed as a stream of counts, each of which hits $M = 1, 2$ bars simultaneously, with a reconstructed energy $E < 100$ MeV. However, single counts produced by high-energy charged particles, interacting with the MCAL either directly, or after interaction with the surroundings, producing secondary particles showers, might be reconstructed with larger multiplicity values $M > 3$ bars and higher energies $E > 100$ MeV. In some cases, when the particle is crossing the detector orthogonally with respect to the satellite axis, a clear particle track can be observed in the detector plane. Figure 4 shows two MCAL data acquisitions, both lasting ~ 16 ms, acquired with the enabled and inhibited AC veto: each small plot represents a single count released in the detector plane YZ , as seen along the X axis, together with its reconstructed energy and hit detector bars. The number of counts acquired with inhibited AC veto is much larger, with respect to the number of counts acquired with enabled AC veto; moreover, some counts are present, hitting a large number of bars ($M \gg 3$ bars) and with extremely high reconstructed energies ($E \gg 100$ MeV), encircled in red.

Those counts, much less frequent in the data acquired with enabled AC veto, are more likely associated with particle events. The plots in Figure 5 show the distribution of $\sim 10^6$ MCAL counts in the $M(E)$ parameter space, with enabled and inhibited AC veto. We can identify a region in this plane where

reconstructed counts are characterized by $M > 3$ bars and $E > 100$ MeV; it is therefore more likely associated with particles. Quantitatively, before the AC shield inhibition, the rate of these counts corresponded to 0.4% of the total background rate, whereas since the AC shield inhibition the counts rose to 6% of the total count rate. For each STE found by our algorithm, we investigate the amount of these “particle-like counts,” with respect to the total number of counts released by the event: this is done in order to establish whether STEs arise from clusters of particle-like counts. The result is that, generally, counts released during STEs are made for $\sim 6\%$ of “particle-like counts,” consistent with the background rate, exhibiting no preference of STEs to be constituted by a larger fraction of these spurious counts.

At the same time, the algorithm searches for short GRB signatures throughout the rebinned light curves. As short GRBs exhibit average durations of $T_{90} \sim 0.3$ s (Kouveliotou et al. 1993) and may last up to $T_{90} \sim 2$ s, they should imply a more complex structure with respect to STE single-bin spikes. As a consequence, the condition for an event to be classified as a candidate GRB is to have a more defined structure of consecutive bins with high significance, either in the 32 ms or the 64 ms timescale considered for the analysis. Obviously, shorter GRBs can occur, and in this case they would release their counts all within a single bin, being identified as STE by the search algorithm. The search for GRBs deals with longer duration signals, with respect to STEs, and require no bin time shifts.

It is important to carry out a cross-check with the GRBs detected by other space missions, in order to validate the burst candidates identified in our search. This is performed by using the GRBs of the InterPlanetary Network (IPN; Hurley & Cline 2004; IPN webpage: <http://www.ssl.berkeley.edu/ipn3/>). Figure 6 shows a short GRB detected by MCAL at UT 2017 Aug 16 14:23:03.89, and identified by the search algorithm as a burst with time duration $T_{90} = 0.26$ s in the 0.4–100 MeV energy range: the burst was confirmed by the close occurrence of the IPN GRB 170816A, detected, among the others, by the *Fermi*-GBM at UT 2017 Aug 16 14:23:03.96, and having a $T_{90} \sim 2$ s in the 50–300 keV energy range (Roberts et al., GCN #21504).

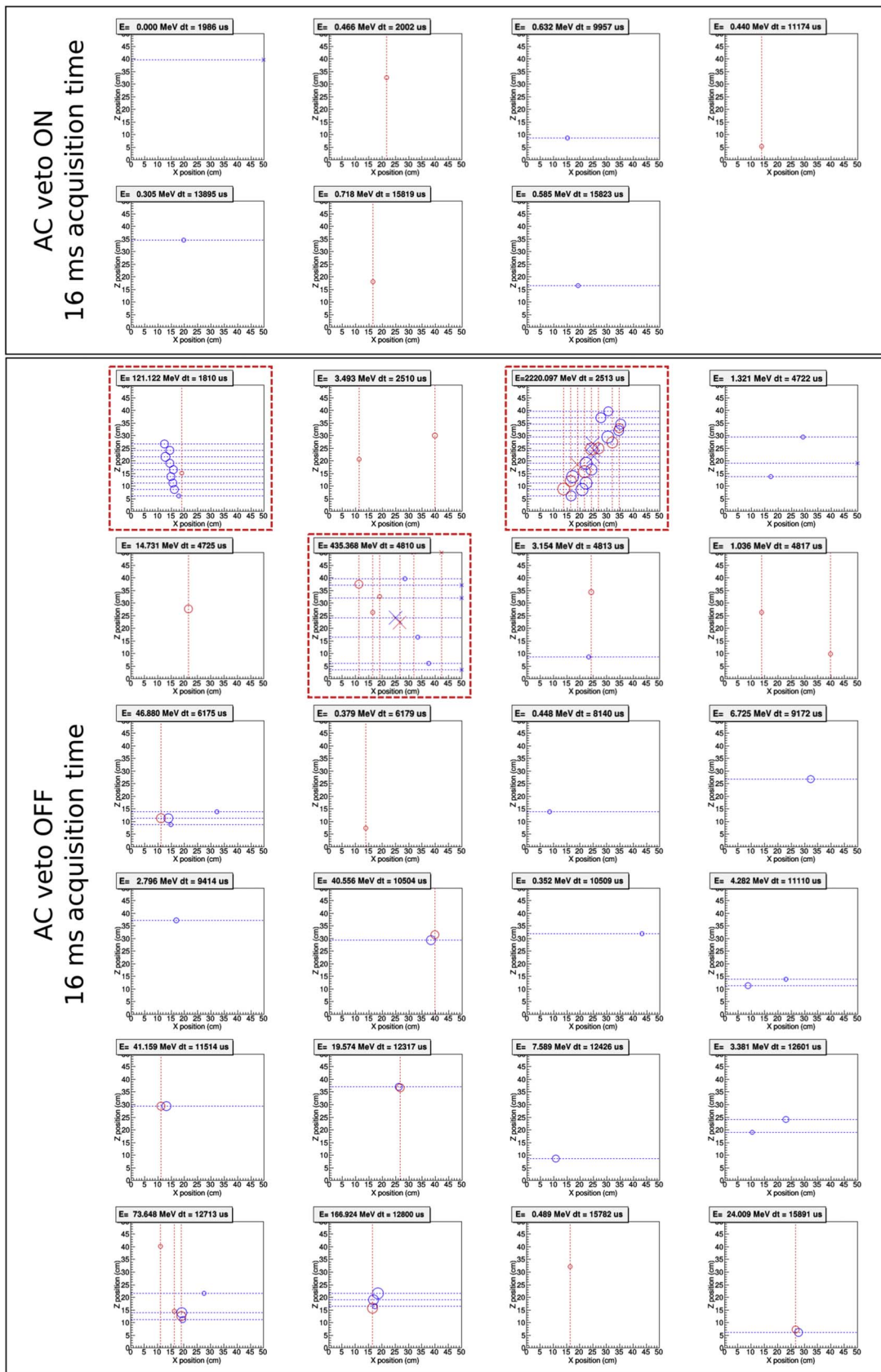


Figure 4. Samples of 16 ms acquisition time, with enabled (upper panel) and inhibited (bottom panel) AC veto: each small plot represents a single count, reconstructed in the MCAL YZ detector plane, as seen along the X axis. Considering the same time interval, the inhibited AC veto makes MCAL detect a larger number of counts, whose reconstructed energy and multiplicity are higher with respect to the enabled AC configuration (encircled in red). Some of these counts also exhibit clear signatures of a particle crossing the detector.

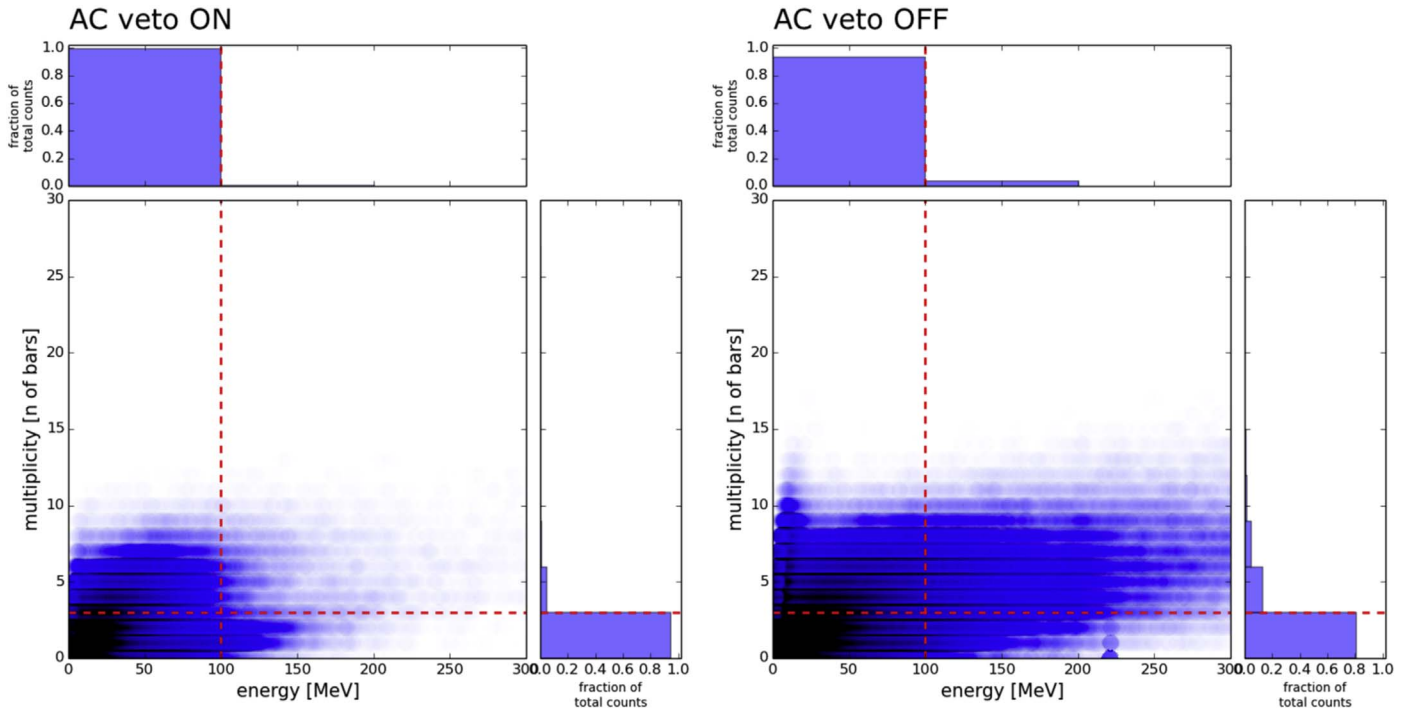


Figure 5. Distribution of $\sim 10^6$ MCAL counts in the energy-multiplicity parameter space, with enabled (left) and inhibited (right) AC veto. The AC shield prevents the detection of a large number of background charged particles, that are mostly concentrated in the $E > 100$ MeV $M > 3$ bars region (delimited by the red dashed lines).

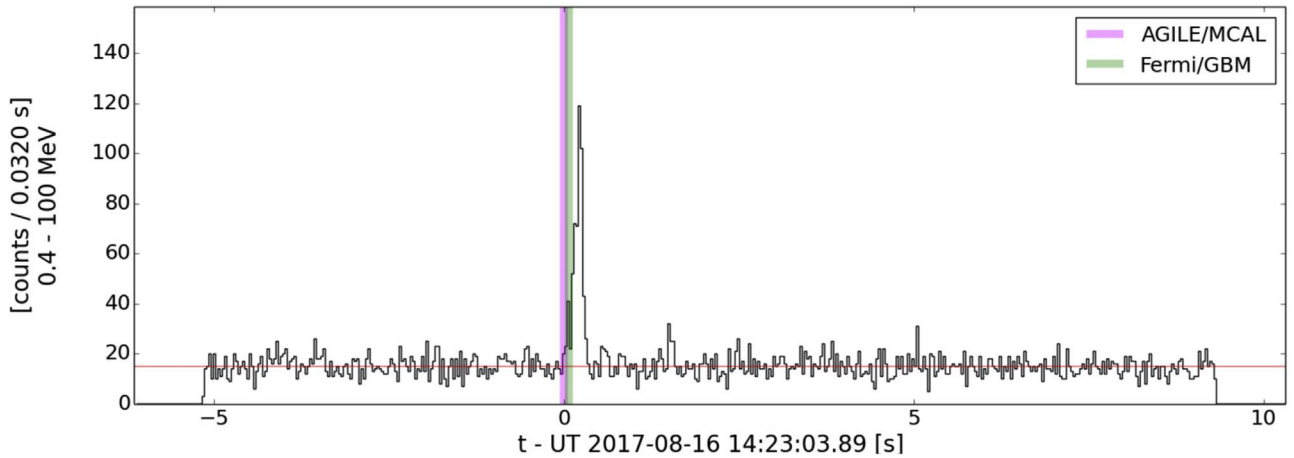


Figure 6. The short GRB 170816A, detected and identified by the MCAL search algorithm at UT 2017 Aug 16 14:23:03.89 (magenta line) as a burst with a duration $T_{90} = 0.27$ s (0.4–100 MeV), and confirmed by the close time association (< 0.07 s) with a burst of the IPN database, detected by the *Fermi*/GBM at UT 2017 Aug 16 14:23:03.96 (green line).

4. Discussion

In the MCAL-GW configuration period (2016 August 1–2018 June 1) the MCAL instrument collected more than 340,000 onboard triggers, for a total acquisition time > 1 day: from the analysis of all data acquisitions, the search for bursts and sub-threshold transients ended up with a total of 52 GRB candidates and more than 26,000 STEs. In order to verify the astrophysical nature of these events, we carried out a cross-check by exploiting the IPN burst database, which consisted of 636 GRBs detected in the same period: we ended up with 40 bursts occurring within ± 10 s from our GRB candidates. We adopted a quite large match time window (20 s), as GRBs can be observed with slightly different light-curve profiles, due to the different sensitivity and

energy range of the detecting instrument: for instance, the previously presented GRB 170816A of Figure 6 was detected by the *Fermi*-GBM [Roberts et al., GCN #21504] with a duration $T_{90} = 2$ s in the 50–300 keV energy band, whereas the MCAL detection shows a sharper time profile lasting only $T_{90} = 0.26$ s, in the 0.4–100 MeV energy band. As the search algorithm does not act on different energy ranges, but only on MCAL full band, it is important not to adopt match time windows for the cross-check that are too tight. We ended up with 40 confirmed GRBs, 17 of which with a $T_{90} < 2$ s and 23 of which with a $T_{90} > 2$ s, in the 0.4–100 MeV energy range. From the related GCN Circulars released for these events, it was possible to classify these events as 30 long GRBs and 10 short GRBs. It is interesting to notice that the distribution of the off-set between MCAL bursts and IPN short

Table 3

Sample of 40 IPN-confirmed GRBs and 12 GRB Candidates, Detected by MCAL in the Period 2016 August 1–2018 June 1, in the MCAL-GW Configuration

Name	Time (UT)	T_{90} (in 0.4–100 MeV)	Other detections
160820A	2016 Aug 20 11:54:10	0.35 s (short)	FE, KW, IN, SW
160821A	2016 Aug 21 20:36:26	>12 s (long)	SW, FE, OPT, KW, CA, AS
160829B	2016 Aug 29 14:18:48	17.66 s (long)	SW, INT, KW
160910A	2016 Sep 10 17:19:46	>14 s (long)	FE, SW, OPT, CA, KW
160911A	2016 Sep 11 14:08:51	>12 s (long)	KW
160927A	2016 Sep 27 18:04:50	0.18 s (short)	SW
161011A	2016 Oct 11 05:13:48	0.19 s (long)	SW, KW
candidate	2016 Nov 6 18:16:18	0.29 s	
161127A	2016 Nov 27 02:49:52	1.70 s (long)	KW
161203A	2016 Dec 3 18:41:07	3.62 s (long)	CA, PO
170115B	2017 Jan 15 17:49:14	>11 s (long)	FE, AS, AG, KW, MO, SW, CA
170127C	2017 Jan 27 01:35:47	0.13 s (short)	FE, AG, AS, PO
170214A	2017 Feb 14 15:34:23	>70 s (long)	FE, KW, SW, OPT
170219A	2017 Feb 19 00:03:07	0.19 s (short)	FE, KW, IN, CA, PO
170308A	2017 Mar 8 05:18:01	5.23 s (long)	FE
170311B	2017 Mar 11 13:45:10	>6 s (long)	KW, MO, SW
candidate	2017 Mar 19 11:58:53	0.12 s	
candidate	2017 Mar 21 17:44:43	1.56 s	
candidate	2017 Mar 24 07:08:53	0.19 s	
170329A	2017 Mar 29 09:17:10	4.86 s (long)	FE, AS, KW
170514A	2017 May 14 04:18:46	0.03 s (long)	FE, CA
candidate	2017 May 20 15:30:23	0.05 s	
170522A	2017 May 22 15:45:27	2.14 s (long)	FE, KW, OPT, IN, MO, SW
170522B	2017 May 22 23:22:02	>8 s (long)	KW, MO, IN
170607B	2017 Jun 7 22:42:04	>6 s (long)	AS, FE, KW, IN, MO
candidate	2017 Jun 13 21:49:07	0.25 s	
candidate	2017 Jun 15 02:41:26	0.51 s	
170616A	2017 Jun 16 16:06:34	0.015 s (short)	KW, MO, IN
170726A	2017 Jul 26 03:46:31	5.76 s (long)	SW, KW
170802A	2017 Aug 2 15:18:26	0.018 s (short)	FE
170816A	2017 Aug 16 14:23:03	0.26 s (short)	FE, KW, SW, CA
170904A	2017 Sep 4 09:45:53	>6 s (long)	HX, IN, SW, KW
170923A	2017 Sep 23 04:31:05	1.92 s (long)	FE
171011A	2017 Oct 11 18:32:46	2.56 s (long)	SW, OPT
171011B	2017 Oct 11 01:05:36	1.66 s (long)	KW, IN, MO, SW
171101A	2017 Nov 1 10:49:51	1.26 s (long)	CA
171103A	2017 Nov 3 23:10:31	1.79 s (short)	SW, FE, KW, AS, IN
candidate	2017 Nov 11 01:11:02	0.03 s	
171119A	2017 Nov 19 23:48:26	>8 s (long)	FE, KW, IN, MO

Table 3
(Continued)

Name	Time (UT)	T_{90} (in 0.4–100 MeV)	Other detections
candidate	2017 Nov 26 15:22:24	0.17 s	
candidate	2017 Dec 20 12:56:12	0.06 s	
171227A	2017 Dec 27 00:00:15	>30 s (long)	AG, FE, KW, AS
180103A	2018 Jan 3 01:08:36	>100 s (long)	SW, AS, KW, OPT
180111A	2018 Jan 11 16:42:06	>6 s (long)	SW, AG, OPT, CA, KW, HX
180204A	2018 Feb 4 02:36:17	0.32 s (short)	SW, OPT
180305A	2018 Mar 5 09:26:16	5.14 s (long)	FE, OPT, KW, SW, CA, AS
180325A	2018 Mar 25 01:54:21	5.28 s (long)	SW, OPT, KW, AS
180326A	2018 Mar 26 03:26:09	0.89 s (long)	KW, IN, MO
180404C	2018 Apr 4 21:42:09	>20 s (long)	CA, KW, MO, IN, AG
candidate	2018 May 15 05:36:07	1.44 s	
candidate	2018 May 17 01:07:16	0.96 s	
180529A	2018 May 29 08:29:12	1.40 s (short)	AG, CA, KW, AS

Table 4
Results from the Spectral Analysis Carried Out for the 10 Short GRBs Detected By MCAL, Whose Localization Was Provided by other Detections

Name	(l,b) (deg)	δ	Flux (erg cm ⁻² s ⁻¹)	Fluence (erg cm ⁻²)	ΔE (MeV)	Red χ^2 (n. dof)
160820A	213.91, 69.43	$2.21^{+1.10}_{-0.53}$	1.27×10^{-6}	0.44×10^{-6}	0.4–10.0	1.21 (48 dof)
160927A	37.63, 31.09	$2.17^{+0.40}_{-0.31}$	2.57×10^{-6}	0.60×10^{-6}	0.4–10.0	1.22 (48 dof)
170127C	325.79, -46.73	$2.21^{+0.17}_{-0.16}$	8.79×10^{-6}	1.22×10^{-6}	0.4–2.0	1.91 (21 dof)
170219A	14.30, 21.17	$1.54^{+0.12}_{-0.12}$	4.18×10^{-6}	0.79×10^{-6}	0.4–10.0	1.70 (48 dof)
170616A	219.81, 8.36	$1.89^{+0.89}_{-0.91}$	2.60×10^{-6}	0.06×10^{-6}	0.4–5.0	1.48 (36 dof)
170802A	243.40, -55.17	$2.16^{+0.23}_{-0.21}$	4.36×10^{-6}	0.08×10^{-6}	0.4–5.0	2.48 (36 dof)
170816A	92.01, -44.67	$2.22^{+0.20}_{-0.18}$	3.03×10^{-6}	0.99×10^{-6}	0.4–10.0	1.26 (48 dof)
171103A	6.75, 23.60	$1.94^{+0.15}_{-0.14}$	6.00×10^{-6}	10.75×10^{-6}	0.4–10.0	1.46 (48 dof)
180204A	84.86, -19.11	$1.79^{+1.15}_{-0.94}$	0.76×10^{-6}	0.24×10^{-6}	0.4–5.0	0.58 ^a (36 dof)
180529A	263.87, -24.64	$2.11^{+0.11}_{-0.10}$	4.37×10^{-6}	6.12×10^{-6}	0.4–10.0	1.32 (48 dof)

Note. All events have been fitted with a single power-law model with photon index δ . The corresponding fluxes and fluences have been calculated on different energy ranges, depending on the spectral shape of each event.

^a This event was analyzed using the XSPEC CSTAT statistic, due to the low number of counts released in the detector by this burst.

GRBs never overcomes 2 s, making the ± 2 s time interval the most reliable matching window for the cross-check with short duration GRBs. The 12 unconfirmed bursts found by our algorithm may represent signatures of short GRBs as well, but it is not possible, on the basis of MCAL data alone, to confirm the real astrophysical nature of these events. All GRBs and GRB candidates are reported in Table 3. Detections of the GRBs are listed with the following acronyms: AGILE (AG), AstroSat-CZTI (AS), CALET (CA), *Fermi* (FE), Insight-HXMT/HE (HX), *INTEGRAL* (IN), KONUS-Wind (KW), Mars Odyssey (MO), POLAR (PO), Optical obs. (OPT), and *Swift* (SW). As illustrated in Figure 2, the MCAL-GW configuration is more sensitive to short duration events and mostly issues ~ 10 s-lasting or 30–40

s-lasting data acquisitions: as a consequence, some long GRBs are not fully covered by MCAL data, and it was not possible to reconstruct the actual whole T_{90} of the event. For these events we only provide a duration lower limit. Longer duration GRBs (e.g., GRB 170214A and GRB 180103A) have triggered more consecutive short data acquisitions, allowing us to provide longer duration lower limits of >70 s and >100 s.

We performed the same cross-search on our STE sample with IPN bursts. For this analysis, we adopted a ± 2 s matching window, that we pointed out earlier as the best matching window for short GRBs. Moreover, a smaller time window reduces the number of expected chance matches, naturally expected due to the large time interval investigated (22 months). The expected number

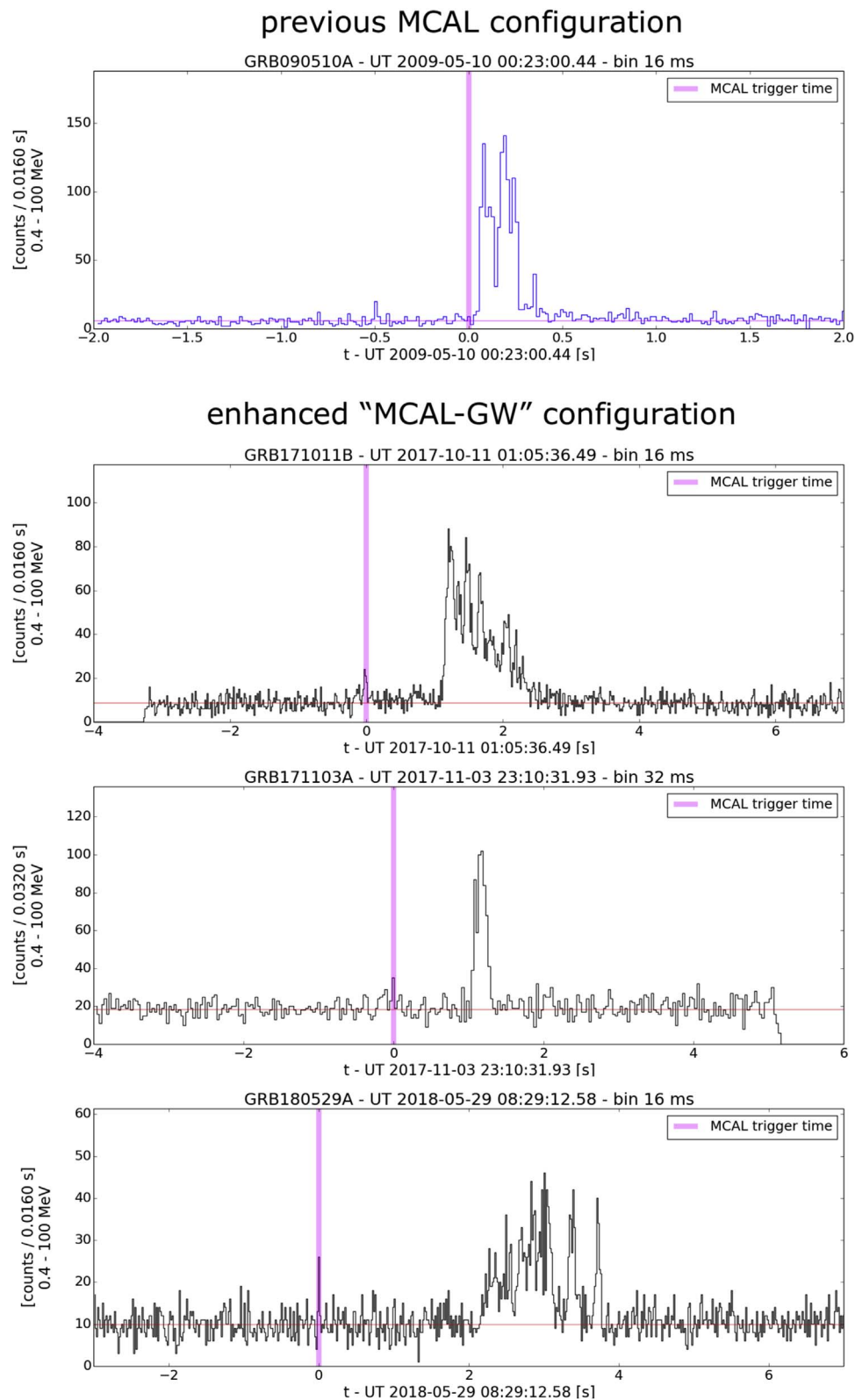


Figure 7. Four short GRBs detected by the AGILE/MCAL. The first burst, (a) GRB 090510A, was anticipated by a weak precursor event ~ 0.5 s before it and was also detected by other satellites; however, the former onboard MCAL configuration was not able to trigger during it, and was only triggered during the on-set of the prompt phase (magenta line). On the contrary, GRB 171011B, (c) GRB 171103A, and (c) GRB 180529A were detected by MCAL running the MCAL-GW configuration: in all these cases, the instrument was triggered during brief and weak anticipating pulses (as seen in the 0.4–100 MeV energy range), providing strong confirmation of the enhanced onboard sensitivity to short duration events.

of events occurring at a rate r in a time window δt is approximately equal to $N_{\text{exp}} \sim r\delta t$, if the rate r at which the event occurs is evaluated over a time interval $T \gg \delta t$. Taking into consideration the total number of STEs $N_{\text{STE}} \sim 26,000$ and IPN GRBs $N_{\text{IPN}} = 636$ observed in a period $T = 22$ months, we obtain the related rates $r_{\text{STE}} = 4.6 \times 10^{-4}$ Hz and $r_{\text{IPN}} = 1.2 \times 10^{-5}$ Hz. Choosing $\delta t = 4$ s $\ll T = 22$ months, the number of expected matches of an STE occurring within δt from an IPN burst will be equal to $N_{\text{exp}} = N_{\text{STE}} \times \delta t \times r_{\text{IPN}} \sim 1.2$.

Our search ended up with no GRBs occurring ± 2 s from the STE events, a result consistent with the expected N_{exp} . However, GRBs of the IPN database are burst transients detected by $n \geq 1$ astrophysical missions, exhibiting well defined light-curve profiles: as a consequence, it is very unlikely for MCAL to detect an IPN burst as a brief single-spike STE. Moreover, the IPN Network database does not constitute a homogenous sample of bursts, as it includes events detected by different missions, with different energy ranges, sensitivities, and orbital positions. A more interesting and promising study would imply the cross-correlation of the AGILE/MCAL STEs with sub-threshold trigger events detected by other space missions, in order to carry out a homogenous search, making use of data acquired by single detectors, such as the *Fermi*/GBM, the *Swift*/BAT, or the *INTEGRAL*/SPI-ACS.

The number of detected short GRBs confirmed by the IPN network is compatible with the number of events detected in the previous MCAL onboard configuration: Galli et al. (2013), in the first MCAL GRB catalog, reported nine short GRBs in close time association with IPN bursts in the AGILE's first two years of life (i.e., ~ 0.4 GRBs/month), compatible with the 10 short GRBs found by AGILE in the first 22 months in the MCAL-GW configuration (i.e., ~ 0.5 GRBs/month). The key point of the new configuration is not given by the number of detected events, but by the enhanced onboard sensitivity to weak high-energy transients: this is confirmed by the way MCAL triggered some short bursts. As shown in the last three plots of Figure 7, for the short GRB 171011B, GRB 171103A, and GRB 180529A, MCAL triggered on short peaks anticipating the main prompt phase burst, confirmed in public light curves acquired by other missions (see GCN #22005 for GRB 171011B, GCN #21998 for GRB 171103A, and GCN #22741 for GRB 180529A). We compare these results with the detection of GRB 090510A (Abdo et al. 2009; Giuliani et al. 2011), a short burst exhibiting brief precursor events occurring 0.5 s before the leading prompt phase (Troja et al. 2010), presented in the first plot of Figure 7: in this case, the burst was detected by MCAL running the previous less sensitive onboard configuration, and the detector was not able to trigger on the 0.5 s anticipating precursor, but only on the on-set of the burst prompt phase.

We performed a spectral analysis of the shortest GRBs detected by MCAL, considering only bursts with a sufficiently high number of counts, reported in Table 4. As the MCAL energy range is lower limited at 400 keV, in most cases, we can investigate only the decreasing highest part of the spectrum: as a consequence, we adopted a simple power-law model $f(E) \sim E^{-\delta}$ to fit the GRB spectral shapes and retrieve the corresponding flux, in different energy ranges, dependent on the burst under analysis. Results of this analysis are provided in Figure 4. Photon indices have a median value of $\delta_{\text{med}} = 2.62$, ranging from 1.79 to 2.63, whereas the corresponding fluences

exhibit values from 0.05×10^{-6} erg cm $^{-2}$ in the [0.4–5.0] MeV energy range to 10.04×10^{-6} erg cm $^{-2}$ in the [0.4–10.0] MeV energy range. All events have been treated with the PGstat XSPEC statistic, based on the maximum likelihood for Poisson data on a Gaussian background, except for GRB 180204A, whose low number of counts required an investigation by means of the XSPEC CSTAT statistic, a modified version of the Cash statistic, for Poisson data on a Poisson background.

The GRBs presented in this study will be treated extensively in the next MCAL GRB catalog, which is currently in preparation.

5. Conclusions

The MCAL detection sensitivity has been increased since 2016 August by changing the onboard trigger configuration to the so-called MCAL-GW configuration. Such a change was aimed at improving the detection of extremely short and weak high-energy transients. Moreover, a new algorithm has been implemented on-ground, to identify short GRBs and to find and manage weak STEs. In the era of gravitational wave detection by the LIGO/Virgo collaboration experiment, and in general of multimessenger astronomy, the detection and prompt identification of short GRBs and other short duration high-energy transients is a key point, as they can represent possible electromagnetic counterparts to gravitational wave events. The preliminary analysis carried out by Verrecchia et al. (2017) for GW170104 was a triggered analysis, targeted on MCAL data acquisition, including the LIGO/Virgo trigger time; on the other hand, this work presents an untriggered analysis, aimed at characterizing criteria to identify sub-threshold triggers in the MCAL data, that can be successively used for cross-checks with other satellites.

MCAL is currently triggering at its highest rate, with ~ 60 triggers/orbit and an average total acquisition time of ~ 600 s/orbit. In the period from 2016 August 1 to 2018 June 1, running the MCAL-GW configuration with enhanced onboard trigger conditions, MCAL detected a total of 52 high-energy bursts, 40 of which were confirmed as genuine GRBs by the cross-check with the IPN bursts database: the confirmed sample consists of 30 long GRBs and 10 short GRBs, whereas 12 other possible short GRBs remain unconfirmed. Moreover, in the same period, MCAL detected more than 26,000 STEs with significance $\geq 6\sigma$, but no events have been found in close time association (± 2 s) with IPN bursts. The detection of three short GRBs, triggered by a weak peak before the main burst, confirms the enhanced trigger detection capability of the instrument to weak events. We foresee the implementation of the MCAL-GW configuration for the LIGO/Virgo O3 run, starting in early 2019.

In this work, we provided a comprehensive picture of the phenomenological features of the STE sample detected by the AGILE MCAL. Nevertheless, the real physical nature of these events remains unclear. Sub-threshold triggers could represent signatures of very short GRBs, as well as those of unrelated astrophysical transients, but they could also be spurious signals due to instrumental noise in the detector, still not clearly identified. Future works that will carry out cross-comparisons with other instruments (e.g., AGILE/MCAL data with *Fermi*/GBM, or *Swift*/BAT, or *INTEGRAL*/SPI-ACS) will constitute a more promising channel of investigation and will surely help answer the question of the origin of STEs.

AGILE is a mission of the Italian Space Agency (ASI), with coparticipation of INAF (Istituto Nazionale di Astrofisica) and INFN (Istituto Nazionale di Fisica Nucleare). This work was carried out in the frame of the ASI-INAF agreement I/028/12/0.

We thank the anonymous referee for the interesting suggestions that substantially improved the quality of our work.

ORCID iDs

Alessandro Ursi  <https://orcid.org/0000-0002-7253-9721>

Marco Tavani  <https://orcid.org/0000-0003-2893-1459>

Francesco Verrecchia  <https://orcid.org/0000-0003-3455-5082>

References

- Abbott, B. P., Abbott, R., Abbott, T. D., et al. 2017a, *PhRvL*, **119**, 161101
- Abbott, B. P., Abbott, R., Abbott, T. D., et al. 2017b, *ApJL*, **848**, L13
- Abbott, B. P., Abbott, R., Abbott, T. D., et al. 2017c, *ApJL*, **848**, L12
- Abdo, A. A., Ackermann, M., Ajello, M., et al. 2009, *Natur*, **462**, 331
- Argan, A., et al. 2004, in IEEE Symposium Conf. Record Nuclear Science, 371
- Baiotti, L., & Rezzolla, L. 2017, *RPPH*, **80**, 096901
- Belczynski, K., Perna, R., Bulik, T., et al. 2006, *ApJ*, **648**, 1110
- Briggs, M. S., Hamburg, R., Veres, P., et al. 2016, *LPICo*, **1962**, 4097
- Burns, E., Connaughton, V., Zhang, B.-B., et al. 2016, *ApJ*, **818**, 110
- Connaughton, V., Goldstein, A. & Fermi GBM—LIGO Group 2017, AAS Meeting, vol 229, 406.08
- Galama, T. J., Vreeswijk, P. M., van Paradijs, J., et al. 1998, *Natur*, **395**, 670
- Galli, M., Marisaldi, M., Fuschino, F., et al. 2013, *A&A*, **553**, A33
- Gehrels, N., & Mészáros, P. 2012, *Sci*, **337**, 932
- Giuliani, A., Cardillo, M., Tavani, M., et al. 2011, *ApJL*, **742**, L30
- Goldstein, A., Veres, P., Burns, E., et al. 2017, *ApJL*, **848**, L14
- Higgins, A. B., Starling, R. L. C., Götz, D., et al. 2017, *MNRAS*, **470**, 314
- Hurley, K., & Cline, T. 2004, in AIP Conf. Ser.727, Gamma-Ray Bursts: 30 Years of Discovery, ed. E. Fenimore & M. Galassi (Melville, NY: AIP), 613
- Klebesadel, R. W., Strong, I. B., & Olson, R. A. 1973, *ApJL*, **182**, L85
- Kocevski, D., Burns, E., Goldstein, A., et al. 2018, *ApJ*, **862**, 152
- Kouveliotou, C., Meegan, C. A., Fishman, G. J., et al. 1993, *ApJL*, **413**, L101
- Labanti, C., Marisaldi, M., Fuschino, F., et al. 2009, *NIMPA*, **598**, 470
- Marisaldi, M., Argan, A., Ursi, A., et al. 2015, *GeoRL*, **42**, 9481
- Marisaldi, M., Fuschino, F., Labanti, C., et al. 2010, *JGRA*, **115**, 0
- Marisaldi, M., Fuschino, F., Tavani, M., et al. 2014, *JGRA*, **119**, 1337
- Mészáros, P., & Rees, M. J. 1993, *ApJ*, **40**, 278
- Nakar, E. 2007, *AdSpR*, **40**, 1224
- Piran, T. 2003, in ASP Conf. Ser.308, From X-ray Binaries to Gamma-Ray Bursts: Jan van Paradijs Memorial Symposium, ed. E. P. van den Heuvel et al. (San Francisco, CA: ASP), 355
- Tavani, M., Barbiellini, G., Argan, A., et al. 2009, *A&A*, **502**, 995
- Troja, E., Rosswog, S., & Gehrels, N. 2010, *ApJ*, **723**, 1711
- Verrecchia, F., Tavani, M., Ursi, A., et al. 2017, *ApJL*, **847**, L20
- Wijers, R. A. M. J., Rees, M. J., & Meszaros, P. 1997, *MNRAS*, **288**, L51